

Equation for Aeroacoustics in a Quiescent Environment

Tapan K. Sengupta^{1†}, Aditi Sengupta¹ and Bhavna Joshi¹

¹Department of Mechanical Engineering, Indian Institute of Technology Dhanbad, Jharkhand-826 004, India.

(Received xx; revised xx; accepted xx)

The perturbation equation for aeroacoustics has been derived in a dissipative medium from the linearized compressible Navier-Stokes equation without any assumption, by expressing the same in spectral plane as in *Continuum perturbation field in quiescent ambience: Common foundation of flows and acoustics* Sengupta *et al.*, *Phys. Fluids*, **35**, 056111 (2023). The governing partial differential equation (PDE) for the free-field propagation of the disturbances in the spectral plane provides the dispersion relation between wavenumber and circular frequency in the dissipative medium, as characterized by a nondimensional diffusion number. Here, the implications of the dispersion relation of the perturbation field in the quiescent medium are probed for different orders of magnitude of the generalized kinematic viscosity, across large ranges of the wavenumber and the circular frequency. The adopted global spectral analysis helps not only classify the PDE into parabolic and hyperbolic types, but also explain the existence of a critical wavenumber depending on space-time scales.

1. Introduction

There is a long precedence of studies on wave propagation in various branches of physics, and yet there is no clear definition of waves, as noted by Whitham (1974). The canonical wave equation was first described by D'Alembert (1750) as,

$$u_{tt} = c^2 u_{xx} \quad (1.1)$$

for the one-dimensional transverse vibration of string in tension. The analytical solution of equation (1.1), subject to initial conditions is available in textbooks (see, e.g., Sengupta (2013) and Sengupta & Bhumkar (2020)), which is characterized by the non-dissipative and non-dispersive nature (i.e. frequency-wavenumber independence) of the solution that is used as a benchmark for developing numerical methods in different branches of engineering and applied physics. For electromagnetic field, Maxwell (1954, 1865) obtained the wave equations for the electric field E , and the magnetic field B , with c as the speed of light in a medium of permeability μ_p and permittivity ϵ_p that fix $c = 1/\sqrt{\mu_p \epsilon_p}$. An electromagnetic wave is transverse in nature, with E and B oscillating perpendicular to the direction of wave propagation.

Other notable wave phenomena governed by equation (1.1) are given in Mulloth *et al.* (2015). The canonical wave equation in acoustics for perturbation pressure is given by Feynman (1965, 1969), based on Euler equation. Similarly, elastic wave propagation in solid mechanics in Whitham (1974) relates applied strain and stress, with the longitudinal displacement u , given by equation (1.1) and $c^2 = E_0/\rho$, where E_0 is the Young's modulus, and ρ is the density of the medium.

The interest in information propagation as sound and flow perturbations arose in a bid to develop an unified description for the disturbance propagation in a dissipative medium, as

† Email address for correspondence: tksengupta@iitism.ac.in

initiated in Sengupta *et al.* (2023). The fundamental governing equation for perturbation pressure in a quiescent medium is given by,

$$\frac{\partial^2 p'}{\partial t^2} = c^2 \nabla^2 p' + \nu_l \frac{\partial}{\partial t} \nabla^2 p' \quad (1.2)$$

where the generalized kinematic viscosity is defined as, $\nu_l = \frac{\lambda + 2\mu}{\rho}$, which includes the effects of the losses during the propagation of the signal either as transverse or as longitudinal waves and/ or diffusive disturbances. The derivation of equation (1.2) does not require the Stokes' hypothesis Stokes (1851); with the first and second coefficient of viscosity contribute to the bulk viscosity for the signal attenuation, specifically for the propagation of acoustic signal as longitudinal wave via compression and dilatation. Equation (1.2) incorporates the first and second coefficients of viscosity via the bulk viscosity defined by $\mu_b = \lambda + \frac{2}{3}\mu$. As reported in Sengupta *et al.* (2023), the effects of bulk viscosity for the propagation of the compression and dilatation waves are included for the onset of the Rayleigh–Taylor instability in Sengupta *et al.* (2022, 2021) showing improved solution of compressible Navier-Stokes equation without invoking the Stokes' hypothesis. Readers interested for a comprehensive review of research on the effects of μ_b are referred to in Sengupta *et al.* (2016) and many other references contained therein. From classical thermodynamic point of view, the Stokes' hypothesis equates the thermodynamic pressure to the mechanical pressure for fluid flow. Furthermore for gases, violation of Stokes' hypothesis is also related to relaxation processes of vibrational modes of the polyatomic medium. Air containing *diatomic nitrogen and oxygen molecules experiences inelastic transfer of energy due to collisions between these molecules, changing the translational energy resulting in changes of the normal stresses*, Sengupta *et al.* (2023). Numerical estimates of μ_b for ideal /noble gases and liquids have been reported in Cramer (2012); Chatwell & Vrabec (2020). Unlike in the Stokes' hypothesis, λ is independent of μ , and that can be orders of magnitude higher in value. Needless to point out that λ and μ are both dissipative, and hence must have positive sign, while Stokes' hypothesis violates this observation. Furthermore, Cramer (2012) has shown that many common fluids and even diatomic gases, display μ_b as thousand times larger than μ .

In deriving equation (1.2), the following polytropic relation between pressure and density perturbations has been presumed,

$$\frac{\partial \rho'}{\partial t} = \frac{1}{c^2} \frac{\partial p'}{\partial t} \quad (1.3)$$

However, for a more generic polytropic processes, one relates the perturbation pressure with the density perturbation as, $p' = K_1 (\rho')^n$. Thus, one can rewrite the above equation by,

$$\frac{\partial p'}{\partial t} = \frac{n}{\gamma} c^2 \frac{\partial \rho'}{\partial t} \quad (1.4)$$

For acoustic signal propagation in a perfect gas, the polytropic index, n , can be considered to lie between one (for isothermal process, as assumed in the beginning erroneously for sound wave propagation) and γ (which is the ratio of specific heats for constant pressure and constant volume processes) for the propagation of acoustic wave as a reversible adiabatic process by neglecting losses and heat transfer. The latter is also associated with the isentropic process assumed for the classical wave equation (1.1). However, the propagation of sound in a dissipative medium, will entail small heat transfer due to losses, and the polytropic index (n) will be different from γ by a small amount. The small departure from isentropic condition stems from the observation for perfect gas, for which the change of entropy across a normal shock wave is known to vary as the cube of the pressure jump across it. In contrast, during the propagation of acoustic signal via compression and dilatation, the associated pressure jump will be negligibly smaller. Thus in

view of reporting the linearized analysis result, one can ignore the difference between n and γ in equation (1.4). Moreover, the dispersive nature of propagating sound waves raises concerns about assuming a single value for the speed of sound.

The propagation of noise in air requires procedures in calculating sound absorbed in standard meteorological condition, such as given by standards issued by SAE in 1975 and ANSI in 1978, whose details are available in Zuckerwar & Meredith (1985). The improved standards were obtained additionally using the concepts of molecular absorption of sound by nitrogen at lower frequencies and vibrational mode of energy exchange between water vapor and oxygen molecules prevalent at higher frequencies.

Studies conducted in the free-field lead to effects of nonstationarity, inhomogeneity and spreading. A comprehensive set of low frequency laboratory measurements needed to identify the relaxation frequency of nitrogen in air was met by Zuckerwar & Meredith (1985) in the experiment performed in a resonant tube. This also provided independent sound absorption measurements overlapping those in dry air, and closing the gap between oxygen relaxation theory and experiment. Thus, one can understand the theoretical properties by studying planar propagation of the perturbation field.

For the one-dimensional planar propagation of the perturbation field, equation (1.2) simplifies to (as given in Blackstock (2000) and derived in Sengupta *et al.* (2023)),

$$\frac{\partial^2 p'}{\partial t^2} - c^2 \frac{\partial^2 p'}{\partial x^2} - v_l \frac{\partial^3 p'}{\partial t \partial x^2} = 0 \quad (1.5)$$

The hydrodynamic and acoustic components of the pressure field are noted over a wide magnitude scales. Thus, it is a challenge to solve simultaneously the flow and acoustic problems. The major contribution in Sengupta *et al.* (2023) is the use of global spectral analysis (GSA) given in Sengupta (2013); Suman *et al.* (2017); Sagaut *et al.* (2023) to classify the wavy and non-wavy nature of the solutions of the space-time dependent PDEs, and is based on the necessary condition of the vanishing of the imaginary part of the amplification factors of the latter for all the physical modes. This classification method for PDEs is different from the classical approach available in textbooks, as in Ames (2014); Sengupta (2004). For the ease of understanding the same, a brief description is provided in the following section.

The paper is formatted in the following manner. In the next section, the analysis of space-time dependent PDEs is described. In section 3, ramifications of this classification are provided for the propagation of acoustic signal in quiescent free-field over an extended ranges of wavenumbers and circular frequencies. Also in this section, the dispersive nature of acoustic signal propagation is further discussed to highlight the difference between the classical wave equation with the space-time dependent perturbation field equation developed and presented here. Specifically, the transformation of the wave equation to diffusion equation across a critical wavenumber is presented in both the sections 3 and 4. The paper closes with a summary and conclusion in section 5.

2. Global Spectral Analysis of space-time dependent PDEs

This is demonstrated with the help of the space-time dependent acoustic signal propagation equation (1.5). This equation arises from the linearized response for free-field propagation in flows and/ or in acoustics. This is presented in the spectral plane by representing the fluctuating pressure by,

$$p'(x, t) = \int \int \hat{p}(k, \omega) e^{i(kx - \omega t)} dk d\omega \quad (2.1)$$

The governing equation (1.5) is represented in the spectral plane by using the above to get the dispersion relation as,

$$\omega^2 + i\nu_l k^2 \omega - c^2 k^2 = 0 \quad (2.2)$$

However, in the framework of GSA, one rewrites the perturbation pressure via the hybrid representation as,

$$p'(x, t) = \int_{Br} \hat{p}(k, t) e^{ikx} dk \quad (2.3)$$

The integral on the right hand side is performed along the Bromwich contour, Br , defined in its strip of convergence as described in van der Pol & Bremmer (1959); Sengupta (2012). For the GSA of the governing equation, a length-scale (L_s) and a time-scale (τ_s) are introduced, so that one can define the physical amplification factor with respect to τ_s and the wavenumber (k) as,

$$G_{1,2}(k, \tau_s) = \frac{\hat{p}(k, t + \tau_s)}{\hat{p}(k, t)} \quad (2.4)$$

To present the results in non-dimensional form, nondimensional wavenumber is introduced as kL_s and a non-dimensional time is introduced by, $N_\tau = c\tau_s/L_s$. If L_s is the smallest resolved length scale, then kL_s will span from zero to the Nyquist limit of π as explained in Sengupta (2013).

Using GSA, one can define the physical amplification factor as in Suman *et al.* (2017) by,

$$G_{1,2}(k, \tau_s) = e^{-i\omega_{1,2}\tau_s} \quad (2.5)$$

where $\omega_{1,2}$ are obtained as the roots of the dispersion relation in equation (2.2), given by,

$$\omega_{1,2} = \frac{-i\nu_l k^2}{2} \pm kcf \quad (2.6)$$

where, $f = \sqrt{1 - \left(\frac{\nu_l k}{2c}\right)^2}$ is the factor that defines the deviation of the dispersion relation from its non-dissipative, isentropic counterpart of the classical wave equation. In GSA, the wavenumber k is the independent variable, and the dispersion relation in equation (2.2), provides the dependence of the circular frequency on k . The complex exponents of the amplification factors indicate corresponding phase shifts given by,

$$\beta_{1,2} = \pm kcf \tau_s \quad (2.7)$$

The positive value of k -dependent f shows the dispersive nature of the dissipative medium, as opposed to the non-dispersive nature of the classical wave equation. The phase speed and the phase shift are related by the nondimensional phase speeds of the acoustic equation as,

$$\frac{c_{ph1,2}}{c} = \frac{\beta_{1,2}}{kc \tau_s} = \pm f \quad (2.8)$$

The corresponding group velocity components ($v_{g1,2}$) of the acoustic equation are obtained as,

$$v_{g1,2} = \frac{d\omega_{1,2}}{dk} = \pm cf \mp \frac{(k\nu_l)^2}{4fc} - i\nu_l k \quad (2.9)$$

An important aspect of this analysis is explained next with the help of the real and imaginary parts of the first physical amplification factor written as,

$$(G_1)_{real} = e^{-\frac{k^2\nu_l}{2}} \cos(kfc\tau_s), \quad (G_1)_{imag} = -e^{-\frac{k^2\nu_l}{2}} \sin(kfc\tau_s) \quad (2.10)$$

These two parts indicate a phase shift over τ_s to be given by β_1 , as noted above. This fixes a phase speed and group velocity over this time interval, as given above.

For a physical system that does not admit *anti-diffusion*, it has been shown in Suman *et al.* (2017) that the imaginary part of $v_{g1,2}$ must be zero. However, for a non-dissipative system: $v_l = 0$, and then the governing equation becomes non-dispersive, with group velocity equal to the phase speed, as is the case for the classical wave equation, with both of these equal to c . Presence of the dissipative term makes the dynamical system diffusion-dominated, and one can define a diffusion number given by, $D_n = v_l \tau_s / L_s^2$.

A typical estimate of non-zero bulk viscosity is given in Sengupta *et al.* (2023), where the general kinematic viscosity has been obtained by the regression analysis of the experimental data in Ash *et al.* (1991). This resulted in $\mu_b = 7.383 \times 10^{-4} + 3.381 \times 10^{-4} T^*$, where T^* is in Kelvin. Considering air at the temperature of 20°C and the corresponding density, dynamic viscosity, one obtains the value of $\lambda/\mu = 9520$. For the analysis presented in a limited region of the (N_τ, kL_s) -plane in Sengupta *et al.* (2023), the properties have been demonstrated for $D_n = 0.14$. In contrast, a detailed analysis is presented here for three values of $D_n = 1.4, 0.14$ and 0.07 in the same region of the (N_τ, kL_s) -plane that brings out important insights on the length- and time-scales' relationship, which shows change of characteristics of the governing PDE from hyperbolic to parabolic type, depending on the length-scale for a fixed time-scale, as explained later for this sub-critical range of wavenumber.

The ramifications of the GSA in classifying space-time dependent PDEs are described in the next section.

3. Characterization of space-time dependent PDEs by GSA

The characterization of the PDE given by equation (1.2) is explained analytically, by inspection of the amplification factors for different length and time scales. These properties are displayed in the (N_τ, kL_s) -plane in the following for the chosen diffusion number D_n , as it was reported in Sengupta *et al.* (2023) for the single case of $D_n = 0.14$ only. This way of representing the property for fixed D_n is advantageous, but the results need careful interpretation, as N_τ and D_n are both functions of τ_s . In the following, properties for three different values of D_n 's are presented here. One notices the fact that the dispersion relation given by equation (2.2) is quadratic, i.e. the dispersion relation for planar wave propagation has two modes.

In figure 1, the properties are shown for the case of a large diffusion number, $D_n = 1.4$, for both the modes. In the top frames, the imaginary part of $G_{1,2}$ are shown for this D_n , as a function of the nondimensional wave number (kL_s), and nondimensional time scale, $N_\tau = c\tau_s/L_s$ combinations. Absence of the imaginary part of $G_{1,2}$ indicates cases when the amplification factor is strictly diffusive. Such a condition is representative of a parabolic PDE, whose amplification factor is strictly real, as shown using GSA in Sengupta (2013). When the amplification factor is complex in the remaining part of (N_τ, kL_s) -plane, the equation (1.2) represents an attenuated wave, which is typical of hyperbolic PDE. From the definition of D_n , N_τ and $k_c = 2c/v_l$, it is readily apparent that $k_c L_s = 2N_\tau/D_n$. Thus, the linear relationship between $k_c L_s$ with N_τ is readily apparent, with the former given as the boundary between the parabolic and hyperbolic PDE regions. This demarcating slanted straight line is clearly noted for both the modes to be identical, with the slope of the straight line inversely proportional to D_n .

In the middle two frames, the two components of the physical phase speed given in equation (2.8) are plotted in the same (N_τ, kL_s) -plane for $D_n = 1.4$, and the region adjacent to the y-axis has the contour value of c_{1ph} equal to zero, that again implies the parabolic nature of the governing PDE, noted for both the modes. In the hyperbolic part of the domains in (N_τ, kL_s) -plane, with the red region indicating a right running wave, and the blue contours indicate left running wave.

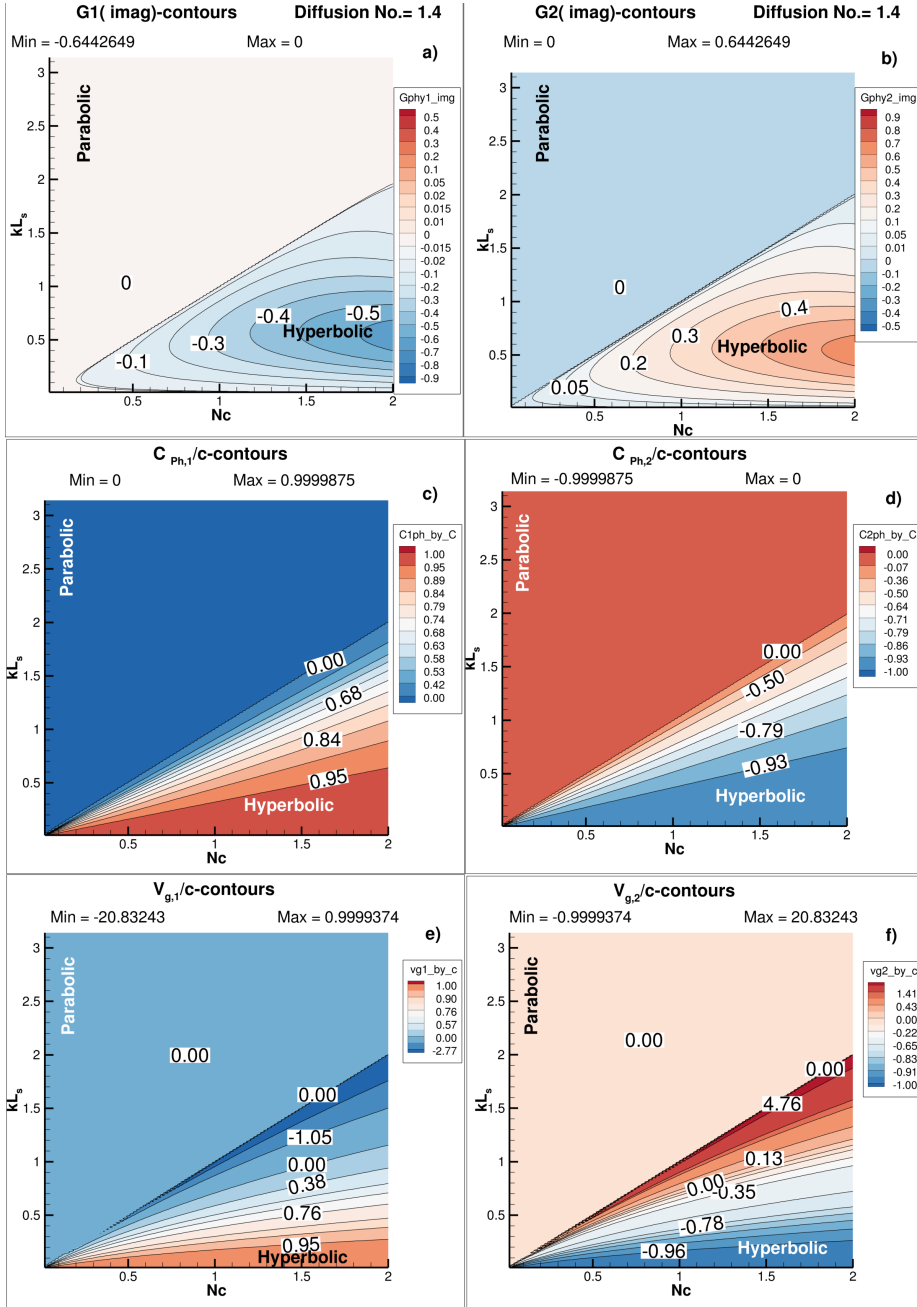


FIGURE 1. The top, middle and bottom frames show for both the modes: imaginary part of the amplification factor, the phase speed, and the group velocity for the diffusion number of $D_n = 1.4$.

In the bottom two frames, the two components of the physical group velocity given in equation (2.9) are plotted in the same (N_τ, kL_s) -plane for $D_n = 1.4$, and the left portion above the k_c -line has the group velocity equal to zero, once again implying the parabolic nature of the governing acoustic equation, noted for both the energy carrying modes. In the hyperbolic part of the region in (N_τ, kL_s) -plane, the red region indicates right running wave and the blue contours

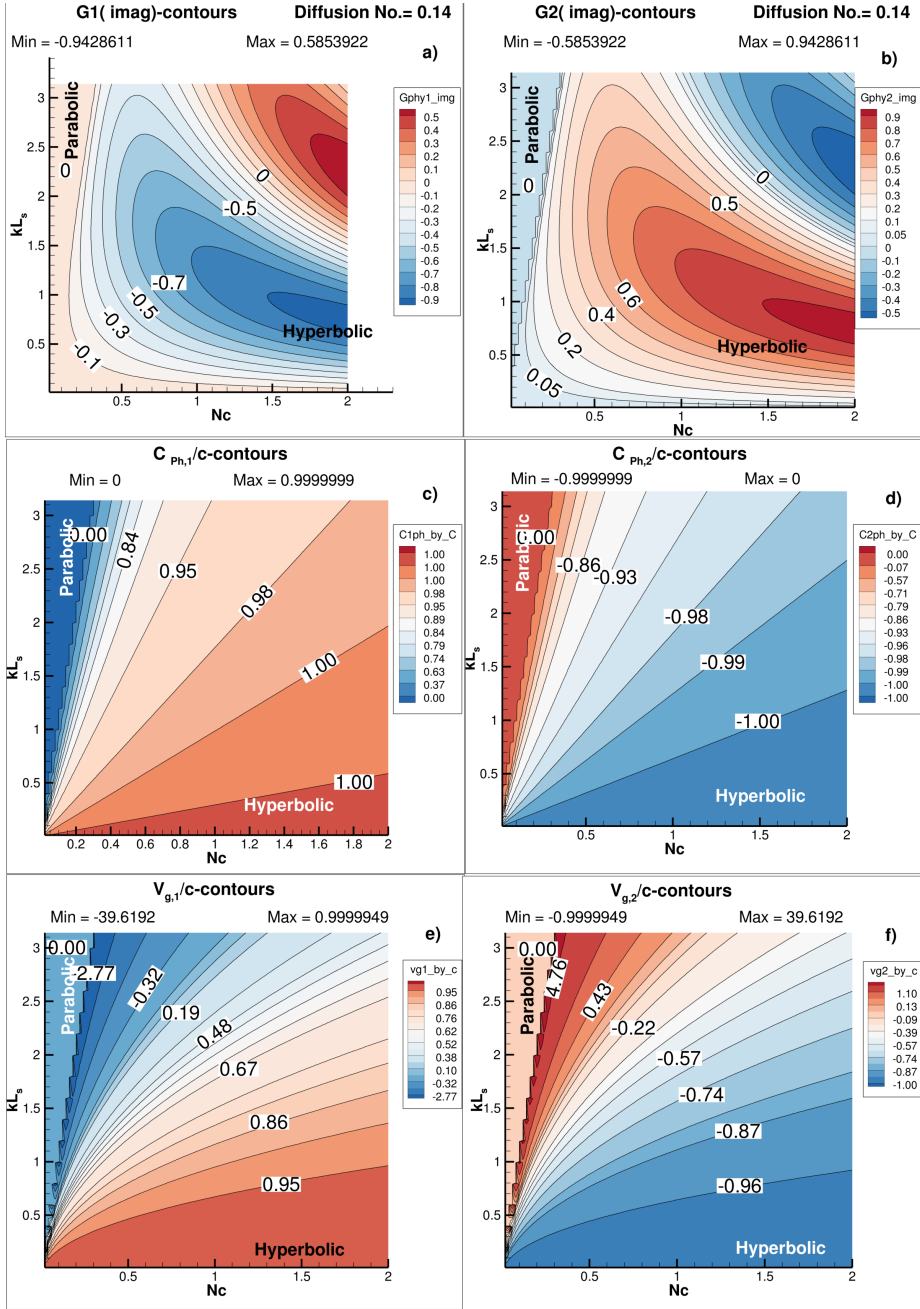


FIGURE 2. The top, middle and bottom frames show for both the modes: imaginary part of the amplification factor, the phase speed, and the group velocity, for the diffusion number of $D_n = 0.14$.

indicate left running wave. The boundary between the parabolic and hyperbolic PDEs are defined from equation (2.6) for which $f = 0$, rendering $\omega_{1,2}$ as strictly imaginary.

In figure 2, the results are shown for the case of $D_n = 0.14$, to compare with the results in figure 1. In the top two frames, the imaginary part of $G_{1,2}$ are shown for this D_n , in the (N_c, kL_s) -plane for identical ranges. As before, absence of the imaginary part helps identify the values of

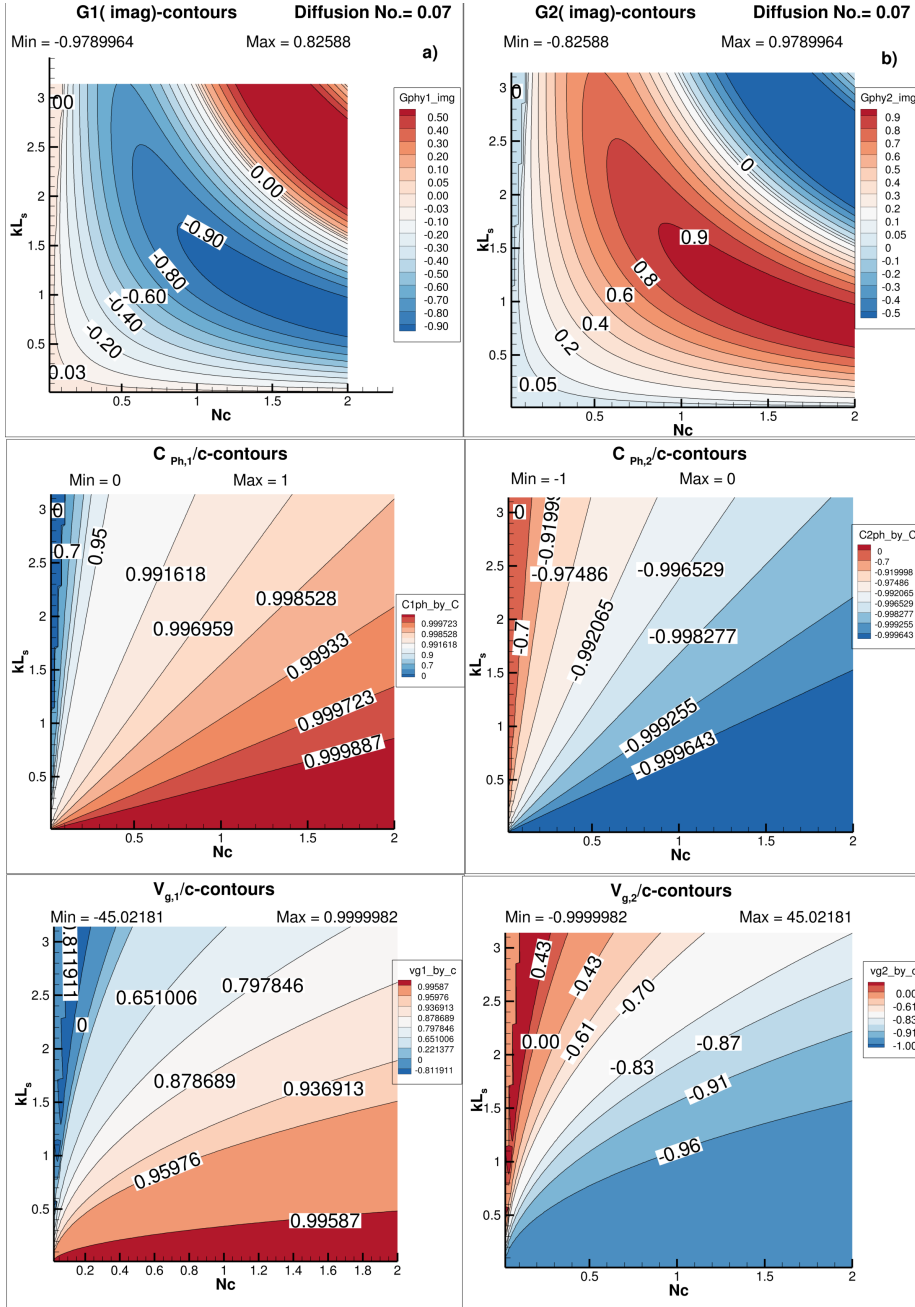


FIGURE 3. The top, middle and bottom frames show for both the modes: imaginary part of the amplification factor, the phase speed, and the group velocity, for the diffusion number of $D_n = 0.07$.

kL_s and N_τ for which the amplification factors are strictly diffusive. From the relation among D_n , N_τ and $k_c L_s$, it is already noted that the demarcating straight line for $k_c L_s$ is sloped more towards the ordinate-axis, for the lower value of D_n in figure 2. These non-dimensional sloping straight lines for the non-dimensional critical cut-off wavenumber are noted for both the modes in the contour plots for the phase speed and the group velocity.

In figure 3, the properties of propagating disturbances are shown for the case of $D_n = 0.07$. Once again, the contour plots of the imaginary part of the amplification factors are shown in the top two frames for both the modes in the (N_τ, kL_s) -plane spanning the same ranges of the abscissa and the ordinate. Due to a further lowered value of D_n , the critical wavenumber given by the $k_c L_s$ -line aligns more closely to the y -axis, as noted in all the six frames of this figure.

For the three values of D_n , it is noted that for the hyperbolic solution the first mode has non-dimensional phase speed ranging between 0 and +1 (right running wave), while the second mode shows this non-dimensional phase speed spanning between -1 to 0 (left running wave). The exact value of zero is noted in the range where the governing PDE is parabolic for both the modes. For the group velocity components, the modes show the wave-packet propagation speed to be zero in the parabolic region of the (N_τ, kL_s) -plane, while the hyperbolic part of the region shows non-zero values spanning between negative and positive values. The first mode displays a large negative value for the group velocity, while the positive value is restricted to +1. The magnitude of the negative group velocity increases with decreasing value of D_n . Similarly, the second mode displays a large positive value, while the negative value is restricted to -1.

3.1. Alternate description of acoustic signal propagation in a dissipative medium

So far, we have noted the role of dissipative medium in propagating perturbation to be determined by the length- and time-scales, in showing the linearized governing PDE to be either parabolic or hyperbolic in nature. This is determined by the dispersion relation. The nature of acoustic signal propagation is further discussed to highlight the difference between the classical wave equation with the space-time dependent perturbation field equation developed here.

In solving equation (1.5) by presenting the properties in terms of the amplification factor (equations (2.4), (2.5)), the modal phase speeds (equation (2.8)), and the modal group velocities (equation (2.9) in figures 1, 2 and 3, we have used non-dimensional length-scale (L_s) and the time-scale (τ_s), with constant diffusion number (D_n) as a parameter. This helped in identifying a critical wavenumber (k_c) line in the non-dimensional (N_τ, kL_s) -plane with its equation given by, $k_c L_s = 2N_\tau/D_n$. While each figure plotted for $D_n = \text{constant}$ contains wealth of data in the hyperbolic region of the domain, lesser information can be gleaned in the parabolic region. Presence of such a transition from the wave equation to a diffusion equation is similar to the conjecture attributed to Kolmogorov length scale for very high Reynolds number convection dominated flow in turbulent regime, as noted in Monin & Yaglom (1971). It has been derived from the first principles in Sengupta *et al.* (2023) and here. However, one also notes the fact that for the constant- D_n plots, each and every point represents a fluid with different generalized viscosity (ν_l). To circumvent these difficulties, it is preferable to represent the properties in the same non-dimensional plane, but for $\nu_l = \text{constant}$ as the parameter. This immediately fixes the cut-off wavenumber given by, $k_c = 2c/\nu_l$ as a horizontal straight line.

For the case considered in Ash *et al.* (1991) with measurements reported for the attenuated acoustic signal, and the case shown in figure 2, one notes $c = 343.11\text{m/s}$ for air at an ambient temperature of 20°C and $\nu_l = 0.1443\text{m}^2/\text{s}$, which fixes the cut-off wavenumber as $k_c = 4755.568\text{m}^{-1}$. The maximum wavenumber (k_{max}) is chosen as four times the value of k_c (which can be chosen arbitrarily, in the absence of any physical data). This, in turn helps one to choose the smallest resolved length-scale in this analysis to be given by $L_s = 3.30485 \times 10^{-4}\text{m}$. For the fixed diffusion number $D_n = 0.14$, this corresponds to the chosen time-scale to be given by, $\tau_s = 1.0596 \times 10^{-7}\text{s}$.

In the following figures, this same value of $L_s = 3.30485 \times 10^{-4}\text{m}$ is used for all the chosen values of ν_l . In the dimensional form, the amplification factors are given by,

$$G_{1,2}(k, \tau_s) = e^{-\nu_l k^2 \tau_s / 2} e^{\mp i k L_s N_\tau \sqrt{1 - (k/k_c)^2}} \quad (3.1)$$

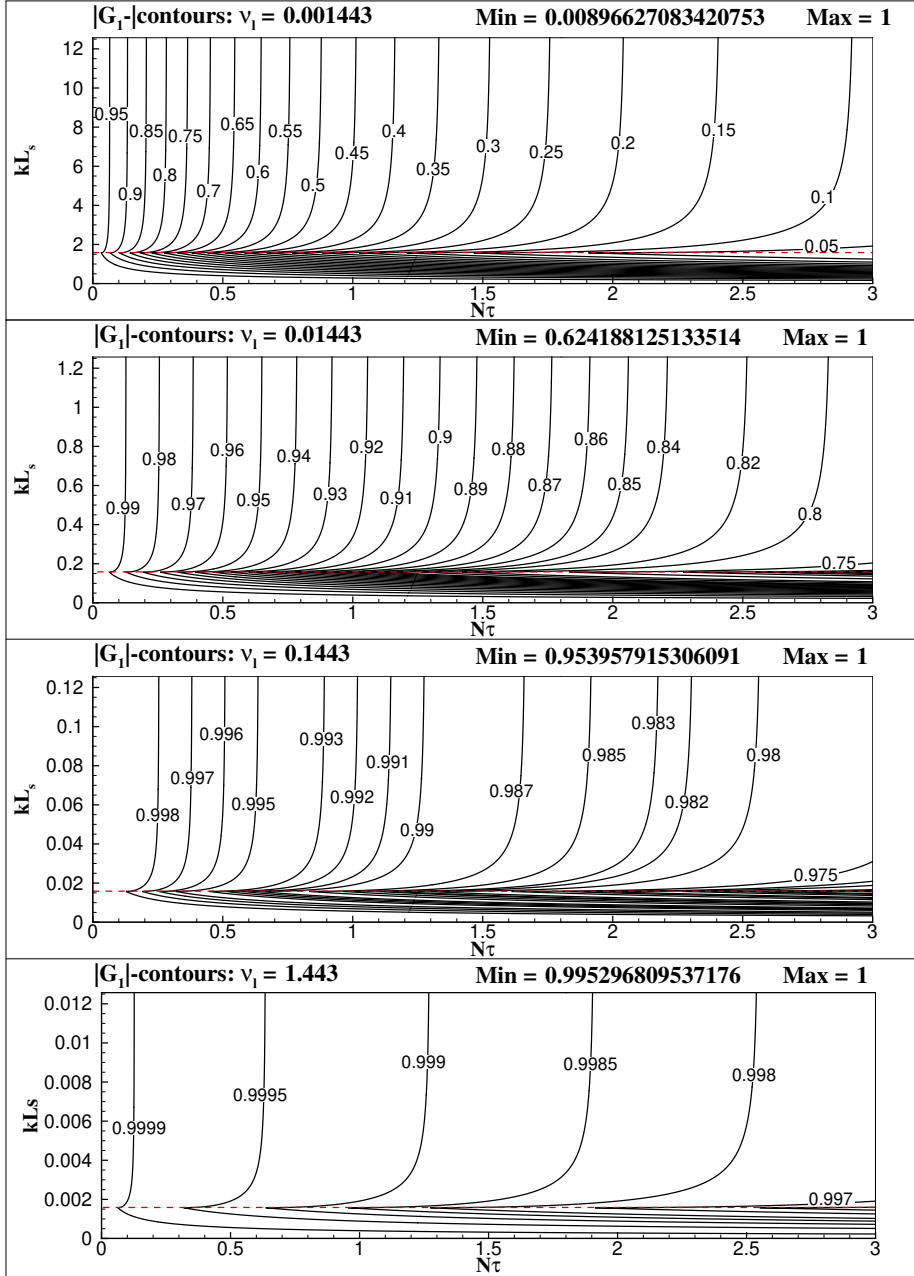


FIGURE 4. The frames show the magnitude of the first mode of the amplification factor for the indicated generalized kinematic viscosity cases in the $(N\tau, kL_s)$ -plane, as given by equation (3.1). The range of nondimensional time scale is arbitrary. The boundary between the regions depicting the diffusion and wave solutions given by the cut-off wavenumber (k_c) is shown by the dotted line (red). The range of nondimensional wavenumber (kL_s) is fixed with $L_s = 3.30485 \times 10^{-4}$ m fixed for the case of $D_n = 0.14$.

The phase speeds are given in the dimensional form as,

$$c_{ph1,2} = \pm c \sqrt{1 - (k/k_c)^2} \quad (3.2)$$

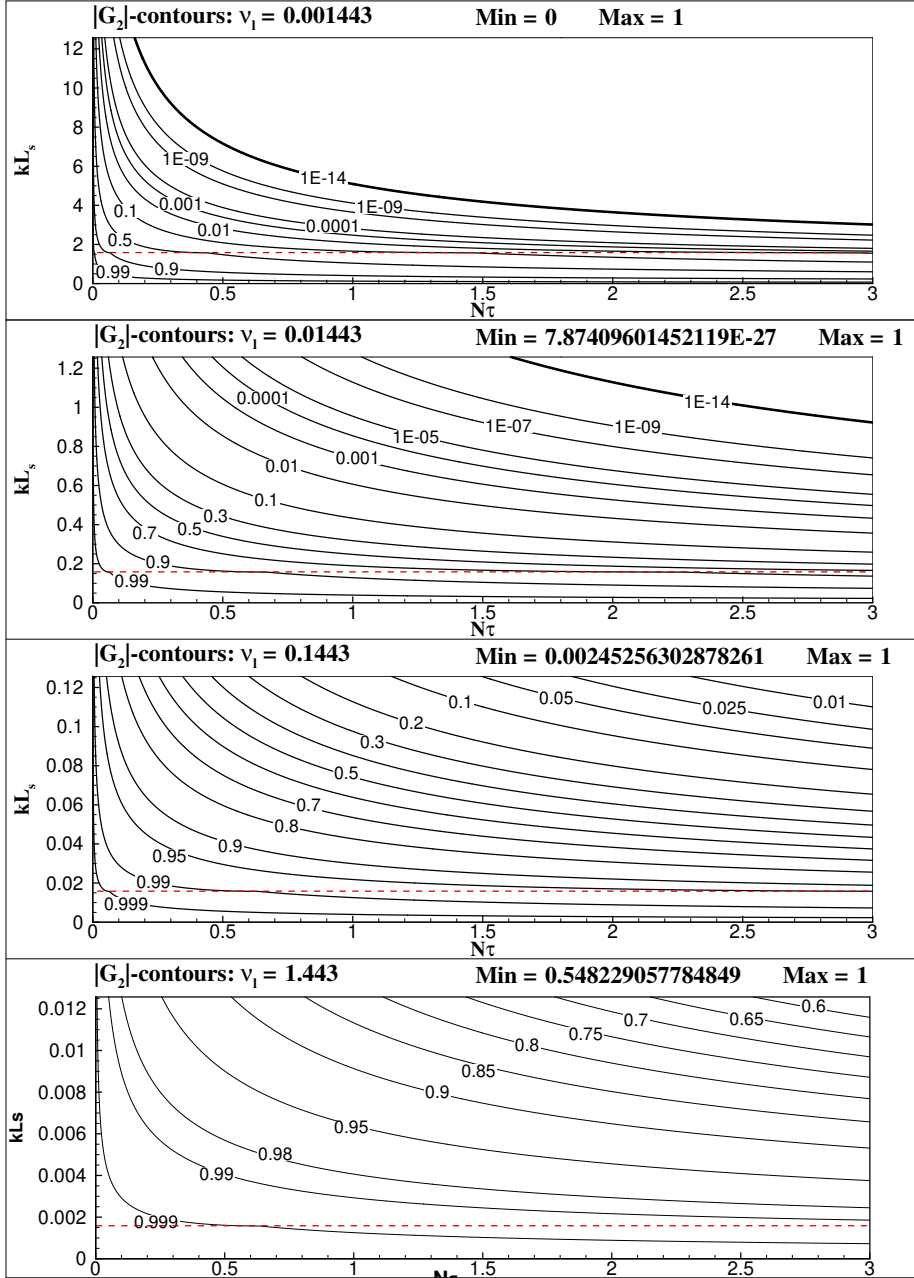


FIGURE 5. The frames show the magnitude of the second mode of the amplification factor for the indicated generalized kinematic viscosity cases in the $(N\tau, kL_s)$ -plane, as given by equation (3.1). The length-scale and time-scale have been chosen as in figure 4. The boundary between the regions depicting the diffusion and wave solutions is given by the non-dimensional cut-off wavenumber $(k_c L_s)$ shown by a dotted line (red).

The corresponding group velocity components are obtained from the real part of the following,

$$v_{g1,2} = \pm c \sqrt{1 - (k/k_c)^2} \mp \frac{(kv_l)^2}{4c \sqrt{1 - (k/k_c)^2}} - iv_l k \quad (3.3)$$

It is readily apparent that the phase speed and the physically relevant group velocity (given strictly by the real part) are not functions of N_τ . It has been noted before as in Suman *et al.* (2017) that the imaginary part of the group velocity gives rise to anti-diffusion, and thus will have no relevance for physical systems which do not admit anti-diffusion. The expressions given in equations (3.1), (3.2) and (3.3) helps one to plot the solution properties in figures 4, 5, 6 and 7 with v_l held as constant.

In figure 4, the modulus of the first amplification factor, $|G_1|$ is shown for the four generalized kinematic viscosity (v_l) cases from 0.001443 to 1.443, each increasing by a factor of ten. It is to be emphasized that one is considering the different magnitudes of the coefficient of viscosity, without even bringing into question the utility of Stokes' hypothesis. In all the frames, the line corresponding to $k_c L_s$ are shown by a dotted (red) line. It is to be noted from equation (3.1) that for $k > k_c$, the exponent in the second factor becomes purely real, thereby augmenting the first attenuating factor and the amplification factor shows the visible discontinuous jump across the $k_c L_s$ -line. For the top frame in figure 4, this occurs for $k L_s = 1.5857$, and in the subsequent frames below, this value is reduced by a factor of ten. Thus, the $k_c L_s$ -line demarcates the mathematical characteristics, where the attenuated wavy solution given by the hyperbolic PDE transforms to the diffusive solution given by the parabolic PDE. In figure 5, the amplitude of the second amplification factor is shown for the same generalized kinematic viscosity cases, which also displays the discontinuity across the $k_c L_s$ -line. Above this line, a very interesting different behavior is noted for the two modes, due to the fact that the second exponent in equation (3.1), apart from becoming real, also becomes of opposite sign. Even though the signal is created in a quiescent ambience, the property of the solution is anisotropic with respect to the spatial dimension. It has its root in the viscous term with mixed derivatives of order three. However, for $k < k_c$, the wavy solution is perfectly symmetric.

In figure 6, the phase speed of the first mode is noted as non-trivial wavy solution for $k < k_c$, while for $k > k_c$, the governing equation becomes diffusive in nature with no variation in phase with time, as the imaginary part of the amplification factor is zero. As the phase speed for the second mode is identical in magnitude, but with opposite in sign, this is not shown. In figure 7, the corresponding group velocity is shown for the first mode, with the regions for different v_l demarcated between the wavy solution and diffusive solution. The second mode also display similar features with identical magnitude, but having opposite sign for the wavy solution. As k approaches the cut-off wavenumber, for a fixed frequency (or N_τ) the group velocity ceases to exist and becomes undefined.

3.2. Multi-modal behavior of the governing equation

If the imaginary part of the physical amplification factor is absent in equation (2.10), then there will be no phase shift in the time interval of τ_s . Such a situation can arise for $\beta_1 = m\pi$, for all integral values of m including zero, i.e.

$$kcf\tau_s = m\pi \quad \text{for } m = 1, 2, \dots, \infty \quad (3.4)$$

For the general case, terming these wavenumbers as k_m , one can rewrite the above condition given by,

$$k_m \sqrt{1 - (k_m/k_c)^2} = \frac{m\pi}{c\tau_s} \quad (3.5)$$

where the cut-off wavenumber is defined by, $k_c = 2c/v_l$, above which $\omega_{1,2}$ becomes strictly imaginary, and then $G_{1,2}(k, \tau_s)$ will be strictly real, as is noted for parabolic PDEs. For $k_m < k_c$, the circular frequency and the physical amplification factor will be complex, and the spatio-

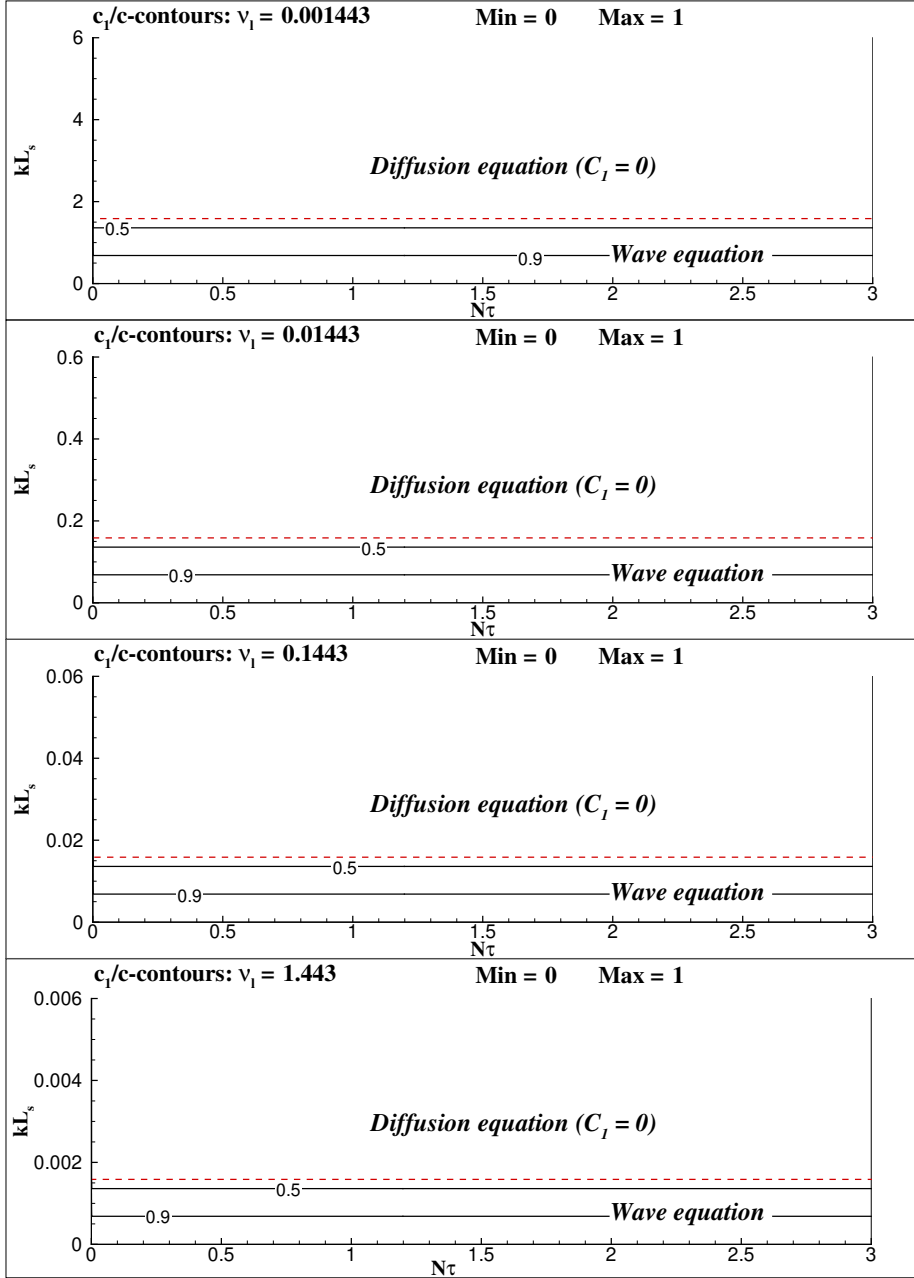


FIGURE 6. The frames show the phase speed of the first mode for the indicated generalized kinematic viscosity cases in the (N_τ, kL_s) -plane, as given by equation (3.2). The length- and time-scales have been chosen as in figure 4. The boundary between the regions depicting the diffusion and wave solutions is given by the non-dimensional cut-off wavenumber ($k_c L_s$) shown by a dotted line (red). The phase speed is defined only in the wave solution range.

temporal dynamics will display an attenuated wave nature, i.e. the governing equation is given by a hyperbolic PDE, with $G_{1,2}$ as complex conjugates.

With the help of the length-scale, L_s , and the non-dimensional time-scale, $N_\tau = \frac{c\tau_s}{L_s}$, the condition given in equation (3.5) can be written alternately as,

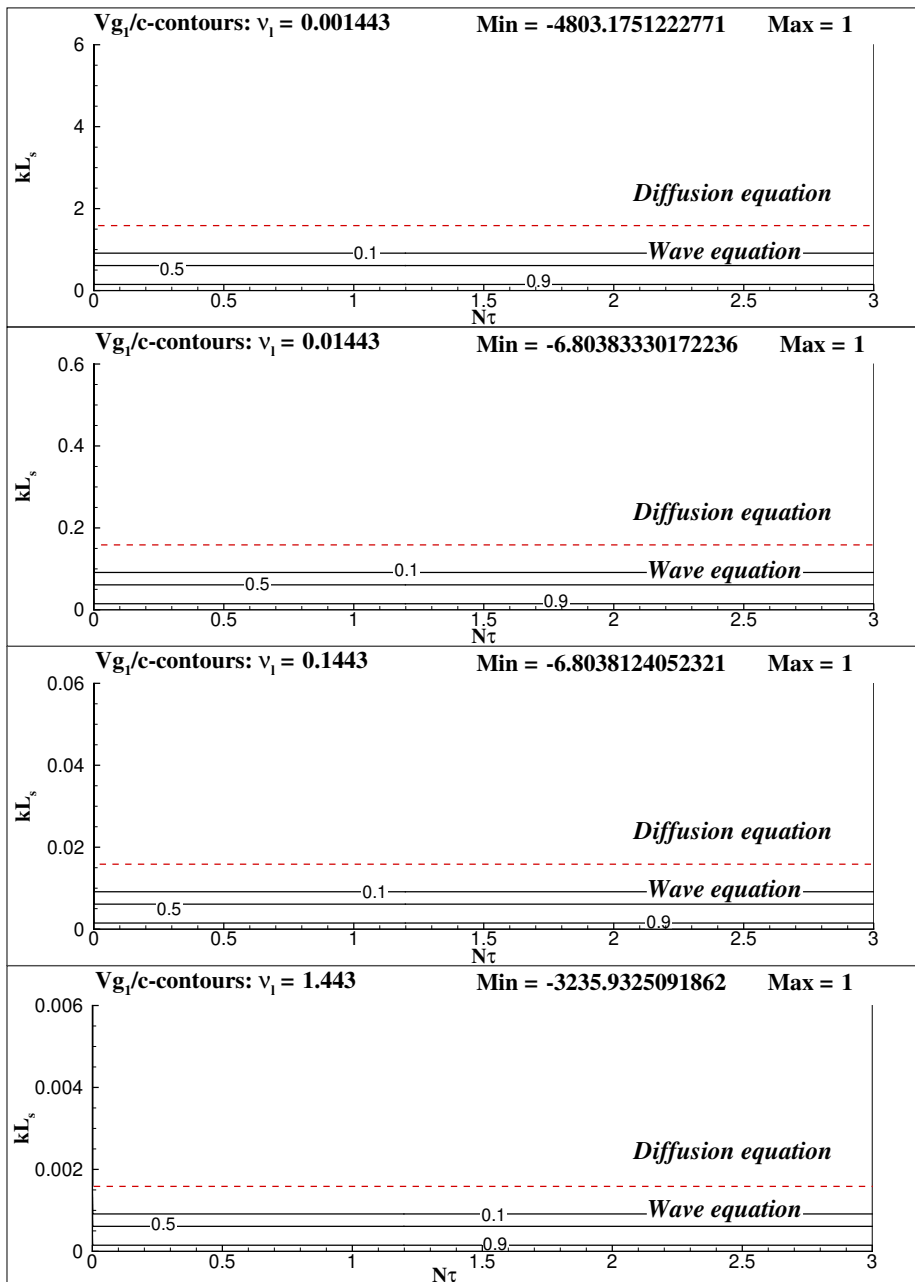


FIGURE 7. The frames show the phase speed of the first mode for the indicated generalized kinematic viscosity cases in the $(N\tau, kL_s)$ -plane, as given by equation (3.2). The length- and time-scales have been chosen as in figure 4. The boundary between the regions depicting the diffusion and wave solutions is given by the non-dimensional cut-off wavenumber ($k_c L_s$) shown by a dotted line (red). The phase speed is defined only in the wave solution range.

$$N\tau k_m L_s \sqrt{1 - (k_m/k_c)^2} = m\pi \quad (3.6)$$

One can plot the loci given by equation (3.6) for different values of m in the $(N\tau, kL_s)$ -plane.

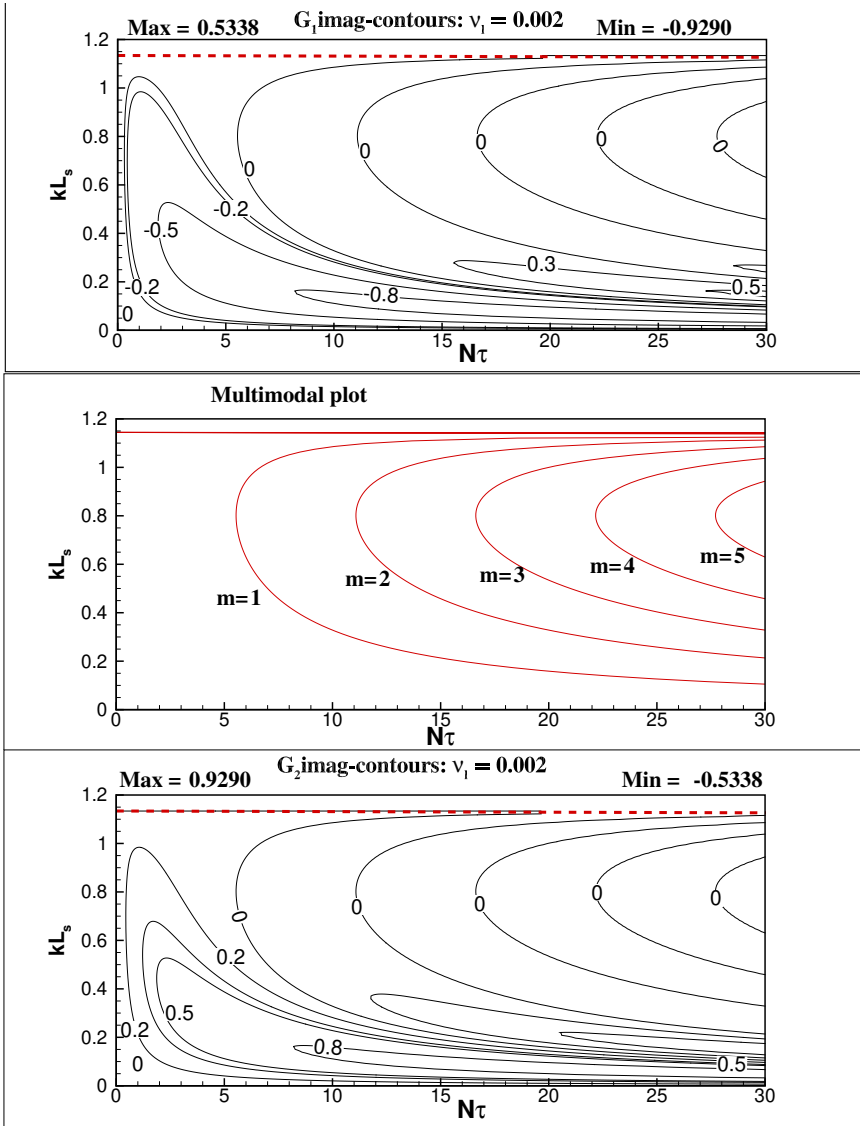


FIGURE 8. The imaginary contours of G_1 (top) and G_2 (bottom) in extended parameter range of $N\tau$ showing multi-modal diffusive nature of the perturbation equation. These modes are obtained using equation (3.6) as shown in the middle frame. For the chosen range of $N\tau$, one can only notice first five modes identified by $m = \text{constant}$ in the figure.

Along these loci, the imaginary part of the amplification factors can be simplified as given next,

$$G_1(k, \tau_s) = e^{-\nu_1 k^2 \tau_s / 2} e^{-im\pi} \quad \text{and} \quad G_2(k, \tau_s) = e^{-\nu_1 k^2 \tau_s / 2} e^{im\pi} \quad (3.7)$$

This clearly shows the amplification factors to be strictly real, where the solution will be diffusive, as it has been shown in figure 8 for different integral values of m . The locus of points in the $(N\tau, kL_s)$ -plane for the subcritical wavenumbers are shown in the middle frame of this figure,

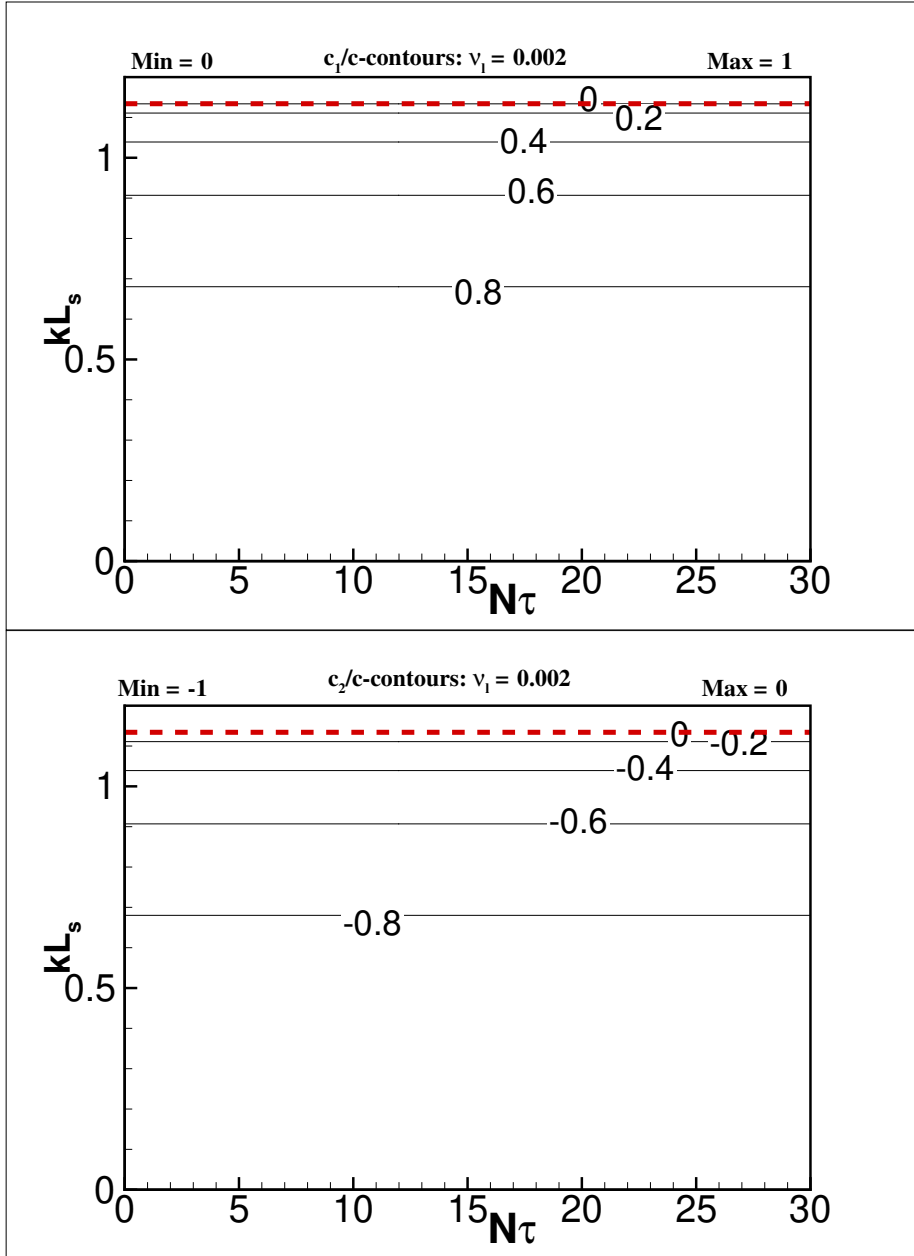


FIGURE 9. The phase speed of both the modes are shown in the extended parameter range of $N\tau$ up to 30. The phase speed remains independent of $N\tau$, and the multi-modal diffusive nature of the perturbation equation noted in figure 8 will not be visible here. The phase speed is given by $\pm(m\pi)/(k\tau_s)$.

that follows equation (3.6). In figure 8, on the top and the bottom frame show the imaginary part of the amplification factors. It can be noted that one observes multi-modal diffusive nature as described in equation (3.7). It implies that solution will be strictly diffusive for multiple such modes for different integer values of m . However, the phase speed will only vanish for $m = 0$. Along the loci of figure 8 shown in the middle frame the phase shift corresponding to $\beta = \pm m\pi$ will give rise to the phase speed given by, $\beta = kc_{1,2}\tau_s$, i.e. $c_{1,2} = \pm(m\pi)/(k\tau_s)$.

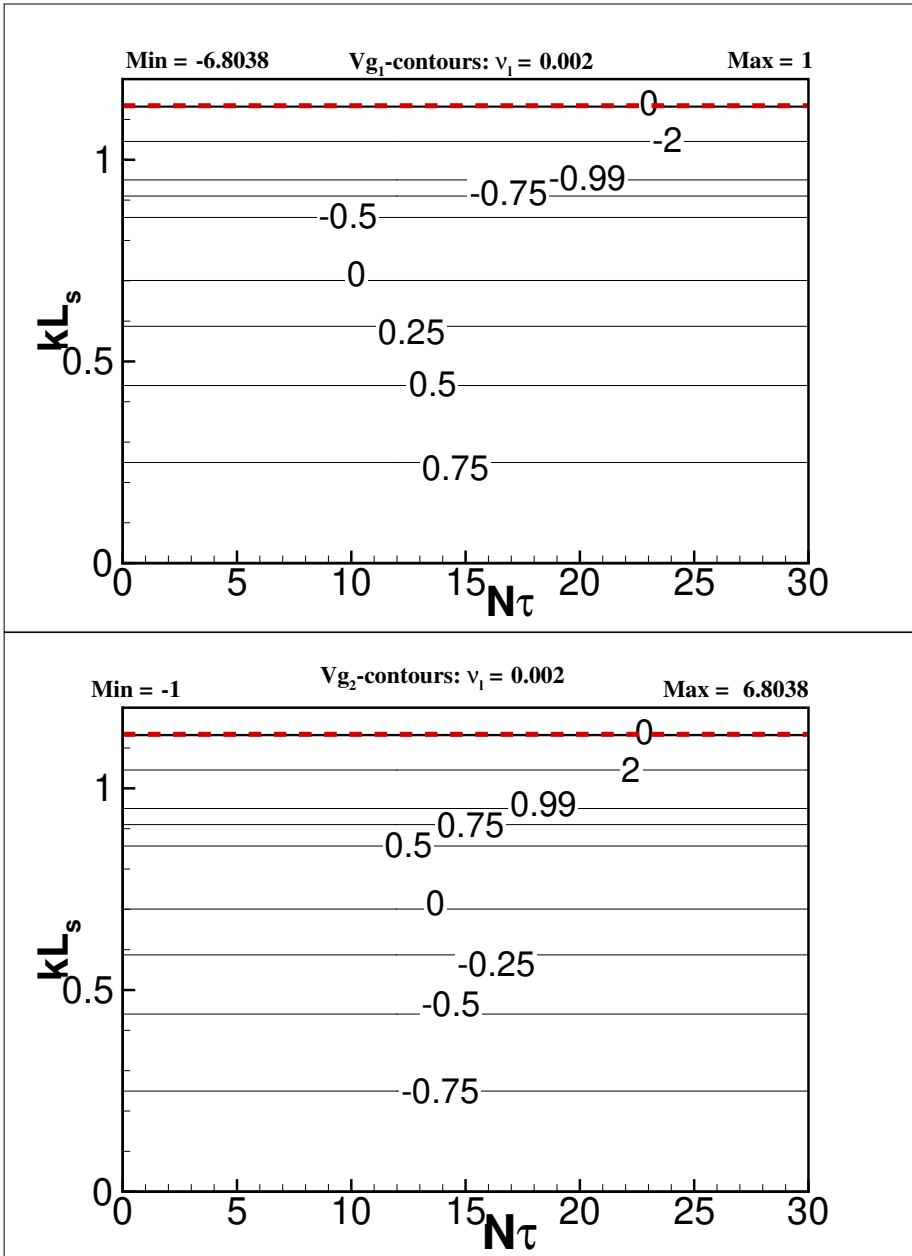


FIGURE 10. The group velocity of both the modes are shown in the extended parameter range of $N\tau$ up to 30. The group velocity is also independent of $N\tau$. The multi-modal diffusive nature of the perturbation equation noted in figure 8 is noted here for two such modes in the plotted contours.

As the phase speed is depicted over the extended time-scale range in figure 9, the corresponding group velocity plots are shown in figure 10. Here also, one notices vanishing values of the group velocity corresponding to two values of kL_s in the figure.

4. Summary and Conclusions

The present work uses of global spectral analysis in the theoretical framework of acoustic disturbance propagation in a quiescent ambience. It is obtained by splitting the field into a mean and its perturbation components and thereafter linearizing the compressible Navier-Stokes equation. The analysis helps one to distinguish between the wave-like propagation of the disturbance and associated diffusion equation depending upon the length scale, for a given time scale. The existence of a cutoff wavenumber, k_c , that demarcates the wave equation and the diffusion equation is a novel feature of the reported research here. This exact quantification for a one-dimensional planar signal, has similarity with the Kolmogorov's length scale which also postulates the conversion of kinetic energy (of the wave equation) to heat energy diffusing at very small scales. The dispersive nature of the governing equation raises the important question about the speed of sound for the dispersive phenomenon. The role of the generalized kinematic viscosity, ν_l is responsible for the observed dispersion and showing the same governing equation to represent wave motion for some lower wavenumber to diffusion at a higher wavenumber and beyond. We also demonstrate further the existence of gaps in the plane constituted by a non-dimensional time scale (N_τ), and nondimensional wavenumber (kL_s) when the governing equation is viewed in the enlarged domain. A multi-modal behavior is noted for such large ranges of the independent variable when one considers fluids with very small values of ν_l . The current research suggests that a careful measurement of the numerical properties of the acoustic wave propagation is essential, especially for ascertaining the roles of phase speed and group velocities of the signal.

REFERENCES

- AMES, W. F. 2014 *Numerical Methods for Partial Differential Equations*. Academic Press, NY, USA.
- ASH, R. L., ZUCKERWAR, A. J. & ZHENG, Z 1991 Second coefficient of viscosity in air. *NASA Technical Reports Server* **19910006051**.
- BLACKSTOCK, D. T. 2000 *Fundamentals of Physical Acoustics*. Wiley-Interscience, Hoboken, New Jersey, USA.
- CHATWELL, R. S. & VRABEC, J. 2020 Bulk viscosity of liquid noble gases. *Journal of Chemical Physics* **152** (9), 094503, arXiv: <https://doi.org/10.1063/1.5142364>.
- CRAMER, M. S. 2012 Numerical estimates for the bulk viscosity of ideal gases. *Physics of Fluids* **24** (6), 066102, arXiv: <https://doi.org/10.1063/1.4729611>.
- D'ALEMBERT, J. L. R 1750 Addition au mémoire sur la courbe que forme une corde tenduë mise en vibration. *Histoire de l'académie royale des sciences et belles lettres de Berlin* **6**, 355–360.
- FEYNMAN, R. P. 1965 The Feynman lectures on physics. *Am. J. Phys.* **33** (9), 750.
- FEYNMAN, R. P. 1969 *Lectures in Physics*. Addison Publishing Co., Addison, USA.
- MAXWELL, J. C. 1865 VIII. A dynamical theory of the electromagnetic field. *Phil. Trans. of the Roy. Soc. London* **155**, 459–512.
- MAXWELL, J. C. 1954 *A Treatise on Electricity and Magnetism*. Dover Publications, New York, USA.
- MONIN, A. S. & YAGLOM, A. M. 1971 *Statistical Fluid Mechanics: Mechanics of Turbulence*. The MIT Press, MA, USA.
- MULLOTH, A., SAWANT, N., HAIDER, I., SHARMA, N. & SENGUPTA, T. K. 2015 High accuracy solution of bi-directional wave propagation in continuum mechanics. *J. Comput. Phys.* **298**, 209–236.
- VAN DER POL, B. & BREMMER, H. 1959 *Operational Calculus based on the Two-Sided Laplace Integral*. Cambridge University Press, Cambridge, UK.
- SAGAUT, P., SUMAN, V. K., SUNDARAM, P., RAJPOOT, M. K., BHUMKAR, Y. G., SENGUPTA, S., SENGUPTA, A. & SENGUPTA, T. K. 2023 Global spectral analysis: Review of numerical methods. *Computers & Fluids* **261**, 105915.
- SENGUPTA, A., SAMUEL, R. J., SUNDARAM, P. & SENGUPTA, T. K. 2021 Role of non-zero bulk viscosity in three-dimensional Rayleigh- Taylor instability: Beyond Stokes' hypothesis. *Comput. Fluids* **225**, 104995.
- SENGUPTA, A., SUNDARAM, P., SUMAN, V. K. & SENGUPTA, T. K. 2022 Three-dimensional direct

- numerical simulation of Rayleigh–Taylor instability triggered by acoustic excitation. *Physics of Fluids* **34** (5), 054108, arXiv: <https://doi.org/10.1063/5.0091109>.
- SENGUPTA, T. K. 2004 *Fundamentals of Computational Fluid Dynamics*. Universities Press, Hyderabad, India.
- SENGUPTA, T. K. 2012 *Instabilities of Flow and Transition to Turbulence*. CRC Press, Boca Raton, USA.
- SENGUPTA, T. K. 2013 *High Accuracy Computing Methods: Fluid Flows and Wave Phenomena*. Cambridge University Press, NY, USA.
- SENGUPTA, T. K. & BHUMKAR, Y. G. 2020 *Computational Aerodynamics and Aeroacoustics*. Springer Singapore, Singapore.
- SENGUPTA, T. K., JHA, S. K., SENGUPTA, A., JOSHI, B. & SUNDARAM, P. 2023 Continuum perturbation field in quiescent ambience: Common foundation of flows and acoustics. *Physics of Fluids* **35** (5), 056111, arXiv: https://pubs.aip.org/aip/pof/article-pdf/doi/10.1063/5.0152037/17611287/056111_1_5.0152037.pdf.
- SENGUPTA, T. K., SENGUPTA, A., SHARMA, N., SENGUPTA, S., BHOLE, A. & SHRUTI, K. S. 2016 Roles of bulk viscosity on Rayleigh–Taylor instability: Non-equilibrium thermodynamics due to spatio-temporal pressure fronts. *Physics of Fluids* **28** (9), 094102, arXiv: <https://doi.org/10.1063/1.4961688>.
- STOKES, G. G. 1851 On the effect of internal friction of fluids on the motion of pendulums. *Trans. Camb. Phil. Soc.* **9** (8), 106.
- SUMAN, V. K., SENGUPTA, T. K., PRASAD, C. J. D., MOHAN, K. S. & SANWALIA, D. 2017 Spectral analysis of finite difference schemes for convection-diffusion equation. *Comput. Fluids* **150**, 95–114.
- WHITHAM, G. B. 1974 *Linear and Nonlinear Waves*. John Wiley & Sons, New York, USA.
- ZUCKERWAR, A. J. & MEREDITH, R. W. 1985 Low-frequency absorption of sound in air. *The Journal of the Acoustical Society of America* **78** (3), 946–955, arXiv: https://pubs.aip.org/asa/jasa/article-pdf/78/3/946/11954284/946_1_online.pdf.